Therefore:

$$\boxed{X_{ss} = \frac{8e^4}{s^2}\big[(p_1\cdot p_3)(p_2\cdot p_4)+(p_1\cdot p_4)(p_2\cdot p_3)\big]}\,. \tag{5.133}$$

Calculation of X_{tt}. For the t-channel:

$$|\mathcal{M}_t|^2 = \frac{e^4}{t^2}\big[\bar u(p_3)\gamma^\nu u(p_1)\big]\big[\bar v(p_2)\gamma_\nu v(p_4)\big]\big[\bar u(p_1)\gamma^\sigma u(p_3)\big]\big[\bar v(p_4)\gamma_\sigma v(p_2)\big]\,. \tag{5.134}$$

Converting to traces (in the $m\to 0$ limit):

$$\frac{1}{4}\sum_{\text{spins}}|\mathcal{M}_t|^2 = \frac{e^4}{4t^2}\,\mathrm{Tr}(\not p_3\gamma^\nu\not p_1\gamma^\sigma)\,\mathrm{Tr}(\not p_2\gamma_\nu\not p_4\gamma_\sigma) \tag{5.135}$$

Following the same procedure as for X_{ss}:

$$\mathrm{Tr}(\not p_3\gamma^\nu\not p_1\gamma^\sigma)\,\mathrm{Tr}(\not p_2\gamma_\nu\not p_4\gamma_\sigma) = 32\big[(p_1\cdot p_2)(p_3\cdot p_4)+(p_1\cdot p_4)(p_2\cdot p_3)\big]\,. \tag{5.136}$$

Therefore:

$$\boxed{X_{tt} = \frac{8e^4}{t^2}\big[(p_1\cdot p_2)(p_3\cdot p_4)+(p_1\cdot p_4)(p_2\cdot p_3)\big]}\,. \tag{5.137}$$

Calculation of X_{st} (interference term). The interference term requires more care. We have:

$$\begin{aligned}-\mathcal{M}_s^*\mathcal{M}_t = -\frac{e^4}{st}&\big[\bar u(p_1)\gamma^\mu v(p_2)\big]\big[\bar v(p_4)\gamma_\mu u(p_3)\big]\\ &\times\big[\bar u(p_3)\gamma^\nu u(p_1)\big]\big[\bar v(p_2)\gamma_\nu v(p_4)\big]\,.\end{aligned} \tag{5.138}$$

To convert this to a trace, we write the product of all four spinor bilinears with explicit indices and use the completeness relations. The key observation is that all spinor indices must be contracted in a single closed loop. Tracing the index chain $\bar u(p_1)\to v(p_2)\to\bar v(p_2)\to v(p_4)\to\bar v(p_4)\to u(p_3)\to\bar u(p_3)\to u(p_1)$ and summing over spins (in the $m\to 0$ limit):

$$\frac{1}{4}\sum_{\text{spins}}\big(-\mathcal{M}_s^*\mathcal{M}_t\big) = -\frac{e^4}{4st}\,\mathrm{Tr}(\not p_1\gamma^\mu\not p_2\gamma_\nu\not p_4\gamma_\mu\not p_3\gamma^\nu)\,. \tag{5.139}$$

This is a trace of eight gamma matrices. We contract the μ indices first using $\gamma^\mu\not a\not b\not c\gamma_\mu = -2\not c\not b\not a$:

$$\mathrm{Tr}(\not p_1\gamma^\mu\not p_2\gamma_\nu\not p_4\gamma_\mu\not p_3\gamma^\nu) = -2\,\mathrm{Tr}(\not p_1\not p_4\gamma_\nu\not p_2\not p_3\gamma^\nu)\,. \tag{5.140}$$

Next, we use $\gamma_\nu \not{a} \not{b} \gamma^\nu = 4(a \cdot b)$:

$$
\begin{aligned}
-2\,\mathrm{Tr}(\not{p}_1 \not{p}_4 \gamma_\nu \not{p}_2 \not{p}_3 \gamma^\nu) &= -2 \cdot 4(p_2 \cdot p_3)\,\mathrm{Tr}(\not{p}_1 \not{p}_4) \\
&= -32\,(p_2 \cdot p_3)(p_1 \cdot p_4)\,.
\end{aligned}
\tag{5.141}
$$

Using $p_2 \cdot p_3 = -u/2$ and $p_1 \cdot p_4 = -u/2$ in the massless limit:

$$
-32 \cdot \frac{u^2}{4} = -8u^2\,. \tag{5.142}
$$

Therefore, in the massless limit this contribution simplifies to:

$$
\frac{1}{4} \sum_{\text{spins}} (-\mathcal{M}_s^* \mathcal{M}_t) = -\frac{e^4}{4st} \cdot (-8u^2) = \frac{2e^4 u^2}{st}\,. \tag{5.143}
$$

To obtain the full interference term, recall from eq. (5.117) that:

$$
X_{st} = -\frac{1}{4} \sum_{\text{spins}} \left(\mathcal{M}_s \mathcal{M}_t^* + \mathcal{M}_s^* \mathcal{M}_t\right). \tag{5.144}
$$

For any complex number z, we have $z + z^* = 2\,\mathrm{Re}(z)$. Applying this with $z = \mathcal{M}_s^* \mathcal{M}_t$:

$$
\mathcal{M}_s \mathcal{M}_t^* + \mathcal{M}_s^* \mathcal{M}_t = (\mathcal{M}_s^* \mathcal{M}_t)^* + \mathcal{M}_s^* \mathcal{M}_t = 2\,\mathrm{Re}(\mathcal{M}_s^* \mathcal{M}_t)\,. \tag{5.145}
$$

Therefore:

$$
X_{st} = -\frac{1}{4} \sum_{\text{spins}} 2\,\mathrm{Re}(\mathcal{M}_s^* \mathcal{M}_t) = -\frac{1}{2} \sum_{\text{spins}} \mathrm{Re}(\mathcal{M}_s^* \mathcal{M}_t) = -\frac{1}{2} \mathrm{Re}\left[\sum_{\text{spins}} \mathcal{M}_s^* \mathcal{M}_t\right], \tag{5.146}
$$

where in the last step we used the linearity of the real part, $\mathrm{Re}(\sum_i z_i) = \sum_i \mathrm{Re}(z_i)$.

Since the trace calculation gives a real result (all scalar products $p_i \cdot p_j$ are real), we can express the interference term directly in Mandelstam variables. In the massless limit this becomes:

$$
\boxed{X_{st} = \frac{4e^4 u^2}{st}}\,. \tag{5.147}
$$

Result in Mandelstam variables. In the center-of-mass frame with $m_e \to 0$, we have:

$$
p_1 = (E, \vec{p}), \qquad p_2 = (E, -\vec{p}) \tag{5.148}
$$

$$
p_3 = (E, \vec{p}\,'), \qquad p_4 = (E, -\vec{p}\,')\,, \tag{5.149}
$$

with $|\vec{p}| = |\vec{p}\,'| = E$ in the massless limit. The Mandelstam variables are:

$$s = (p_1 + p_2)^2 = 4E^2 \tag{5.150}$$
$$t = (p_1 - p_3)^2 = -2E^2(1 - \cos\theta) \tag{5.151}$$
$$u = (p_1 - p_4)^2 = -2E^2(1 + \cos\theta)\,, \tag{5.152}$$

where θ is the scattering angle. They satisfy $s + t + u = 0$ (for massless particles).

The scalar products become:

$$p_1 \cdot p_2 = \frac{s}{2}, \qquad p_3 \cdot p_4 = \frac{s}{2} \tag{5.153}$$
$$p_1 \cdot p_3 = -\frac{t}{2}, \qquad p_2 \cdot p_4 = -\frac{t}{2} \tag{5.154}$$
$$p_1 \cdot p_4 = -\frac{u}{2}, \qquad p_2 \cdot p_3 = -\frac{u}{2}\,. \tag{5.155}$$

Substituting into eqs. (5.133), (5.137), and (5.147):

$$X_{ss} = \frac{8e^4}{s^2}\left[\frac{t^2}{4} + \frac{u^2}{4}\right] = \frac{2e^4}{s^2}(t^2 + u^2) \tag{5.156}$$
$$X_{tt} = \frac{8e^4}{t^2}\left[\frac{s^2}{4} + \frac{u^2}{4}\right] = \frac{2e^4}{t^2}(s^2 + u^2) \tag{5.157}$$
$$X_{st} = \frac{4e^4u^2}{st}\,. \tag{5.158}$$

The total spin-averaged amplitude squared is:

$$\boxed{\overline{|\mathcal{M}|^2} = 2e^4\left[\frac{t^2 + u^2}{s^2} + \frac{s^2 + u^2}{t^2} + \frac{2u^2}{st}\right]}\,. \tag{5.159}$$

Differential cross section. We now derive the differential cross section from $\overline{|\mathcal{M}|^2}$, showing every step explicitly. The starting point is the BD master formula (3.55):

$$d\sigma = \frac{1}{\mathcal{F}}\left(\prod_{i\in\text{fermions}} 2m_i\right)\overline{|\mathcal{M}_{\text{BD}}|^2}\,d\Phi_2\,. \tag{5.160}$$

As shown for $e^+e^- \to \mu^+\mu^-$ (eq. (5.72)), the factor $\prod(2m_i)$ cancels the $1/(2m)^2$ from the BD spin sums, so the net result is equivalent to using:

$$d\sigma = \frac{1}{\mathcal{F}}\overline{|\mathcal{M}|^2}\,d\Phi_2\,, \tag{5.161}$$

where $\overline{|\mathcal{M}|^2}$ denotes the trace expression *without* the $1/(2m)^2$ prefactors.

We now evaluate the flux factor $\mathcal{F}$ and the two-body phase space $d\Phi_2$ in the CM frame.

Step 1: The flux factor. By definition (eq. (3.53)), $\mathcal{F} = 4\sqrt{(p_1 \cdot p_2)^2 - m_1^2 m_2^2}$. In the CM frame, $\vec{p}_1 + \vec{p}_2 = 0$, so $p_1 = (E_1, \vec{p})$ and $p_2 = (E_2, -\vec{p})$. Then:

$$p_1 \cdot p_2 = E_1 E_2 + |\vec{p}|^2 . \tag{5.162}$$

Also $s = (p_1 + p_2)^2 = (E_1 + E_2)^2$, so $E_1 + E_2 = \sqrt{s}$. Computing:

$$\begin{aligned}(p_1 \cdot p_2)^2 - m_1^2 m_2^2 &= (E_1E_2 + |\vec{p}|^2)^2 - (E_1^2 - |\vec{p}|^2)(E_2^2 - |\vec{p}|^2) \\ &= E_1^2E_2^2 + 2E_1E_2|\vec{p}|^2 + |\vec{p}|^4 - E_1^2E_2^2 + (E_1^2 + E_2^2)|\vec{p}|^2 - |\vec{p}|^4 \\ &= (2E_1E_2 + E_1^2 + E_2^2)\,|\vec{p}|^2 = (E_1 + E_2)^2\,|\vec{p}|^2 = s\,|\vec{p}|^2 .\end{aligned} \tag{5.163}$$

Therefore:

$$\mathcal{F} = 4\sqrt{s}\,|\vec{p}|\,. \tag{5.164}$$

Step 2: The two-body phase space $d\Phi_2$. The Lorentz-invariant n-body phase space (eq. (3.45)) for $n = 2$ reads:

$$d\Phi_2 = (2\pi)^4\,\delta^{(4)}(p_1 + p_2 - p_3 - p_4)\,\frac{d^3p_3}{(2\pi)^3\,2E_3}\,\frac{d^3p_4}{(2\pi)^3\,2E_4}\,. \tag{5.165}$$

We evaluate this in the CM frame where $\vec{p}_1 + \vec{p}_2 = 0$, so the delta function enforces $\vec{p}_3 + \vec{p}_4 = 0$ and $E_3 + E_4 = \sqrt{s}$.

Integrate over $\vec{p}_4$: the three-momentum delta function $\delta^{(3)}(\vec{p}_3 + \vec{p}_4)$ sets $\vec{p}_4 = -\vec{p}_3$, removing d^3p_4 and one factor of $(2\pi)^3$:

$$d\Phi_2 = \frac{(2\pi)^4}{(2\pi)^6}\,\delta(E_3 + E_4 - \sqrt{s})\,\frac{d^3p_3}{2E_3 \cdot 2E_4}\bigg|_{\vec{p}_4 = -\vec{p}_3} = \frac{1}{4\pi^2}\,\delta(E_3 + E_4 - \sqrt{s})\,\frac{d^3p_3}{4E_3E_4}\,. \tag{5.166}$$

Switch to spherical coordinates: write $d^3p_3 = |\vec{p}\,'|^2\,d|\vec{p}\,'|\,d\Omega$ where $|\vec{p}\,'| \equiv |\vec{p}_3|$ and $d\Omega = \sin\theta\,d\theta\,d\varphi$:

$$d\Phi_2 = \frac{1}{16\pi^2}\,\delta(E_3 + E_4 - \sqrt{s})\,\frac{|\vec{p}\,'|^2\,d|\vec{p}\,'|}{E_3E_4}\,d\Omega\,. \tag{5.167}$$

Integrate over $|\vec{p}\,'|$: the remaining delta function fixes $|\vec{p}\,'|$ via $E_3(|\vec{p}\,'|) + E_4(|\vec{p}\,'|) = \sqrt{s}$, where $E_i = \sqrt{|\vec{p}\,'|^2 + m_i^2}$. To evaluate this, we need:

$$\frac{d(E_3 + E_4)}{d|\vec{p}\,'|} = \frac{|\vec{p}\,'|}{E_3} + \frac{|\vec{p}\,'|}{E_4} = |\vec{p}\,'|\,\frac{E_3 + E_4}{E_3E_4} = |\vec{p}\,'|\,\frac{\sqrt{s}}{E_3E_4}\,, \tag{5.168}$$

where in the last step we used $E_3 + E_4 = \sqrt{s}$ (imposed by the delta function). Therefore:

$$\delta(E_3 + E_4 - \sqrt{s}) = \frac{E_3 E_4}{|\vec{p}\,'|\sqrt{s}}\,\delta(|\vec{p}\,'| - |\vec{p}\,'|_0)\,, \tag{5.169}$$

where $|\vec{p}\,'|_0$ is the value satisfying the energy constraint. Substituting into (5.167) and integrating over $|\vec{p}\,'|$:

$$d\Phi_2 = \frac{1}{16\pi^2}\frac{|\vec{p}\,'|^2}{E_3 E_4} \cdot \frac{E_3 E_4}{|\vec{p}\,'|\sqrt{s}}\,d\Omega = \frac{|\vec{p}\,'|}{16\pi^2\sqrt{s}}\,d\Omega\,. \tag{5.170}$$

Step 3: Combining flux and phase space. Substituting (5.164) and (5.170) into (5.161):

$$\frac{d\sigma}{d\Omega} = \frac{1}{4\sqrt{s}\,|\vec{p}\,|} \cdot \frac{|\vec{p}\,'|}{16\pi^2\sqrt{s}}\,\overline{|\mathcal{M}|^2} = \frac{|\vec{p}\,'|}{64\pi^2 s\,|\vec{p}\,|}\,\overline{|\mathcal{M}|^2}\,. \tag{5.171}$$

This is the **general** $2 \to 2$ **CM-frame cross section**, valid for arbitrary masses.

Step 4: Ultrarelativistic limit. For $m_e \to 0$ (Bhabha scattering at $\sqrt{s} \gg m_e$), both initial and final particles are effectively massless: $|\vec{p}\,| = |\vec{p}\,'| = E = \sqrt{s}/2$. Therefore $|\vec{p}\,'|/|\vec{p}\,| = 1$ and:

$$\boxed{\frac{d\sigma}{d\Omega} = \frac{1}{64\pi^2 s}\,\overline{|\mathcal{M}|^2}}\,. \tag{5.172}$$

Substituting eq. (5.159) and using $e^4 = (4\pi\alpha)^2 = 16\pi^2\alpha^2$:

$$\begin{aligned}\frac{d\sigma}{d\Omega} &= \frac{1}{64\pi^2 s} \cdot 2e^4\left[\frac{t^2+u^2}{s^2} + \frac{s^2+u^2}{t^2} + \frac{2u^2}{st}\right] \\ &= \frac{2 \cdot 16\pi^2\alpha^2}{64\pi^2 s}\left[\frac{t^2+u^2}{s^2} + \frac{s^2+u^2}{t^2} + \frac{2u^2}{st}\right].\end{aligned} \tag{5.173}$$

Therefore:

$$\boxed{\frac{d\sigma}{d\Omega} = \frac{\alpha^2}{2s}\left[\frac{t^2+u^2}{s^2} + \frac{s^2+u^2}{t^2} + \frac{2u^2}{st}\right]}\,. \tag{5.174}$$

This is the Bhabha cross section in Lorentz-invariant form. Note the three contributions: s-channel ($\propto 1/s^2$), t-channel ($\propto 1/t^2$), and interference ($\propto 1/(st)$).

Angular distribution. To express (5.174) in terms of the scattering angle θ, we substitute the CM-frame Mandelstam variables $t = -\frac{s}{2}(1-\cos\theta)$ and $u =$

$-\frac{s}{2}(1+\cos\theta)$. Each ratio becomes:

$$\frac{t^2+u^2}{s^2} = \frac{s^2(1-\cos\theta)^2/4 + s^2(1+\cos\theta)^2/4}{s^2} = \frac{1}{2}(1+\cos^2\theta)\,, \tag{5.175}$$

$$\frac{s^2+u^2}{t^2} = \frac{s^2+s^2(1+\cos\theta)^2/4}{s^2(1-\cos\theta)^2/4} = \frac{4+(1+\cos\theta)^2}{(1-\cos\theta)^2}\,, \tag{5.176}$$

$$\frac{2u^2}{st} = \frac{2\cdot s^2(1+\cos\theta)^2/4}{s\cdot[-s(1-\cos\theta)/2]} = -\frac{(1+\cos\theta)^2}{1-\cos\theta}\,. \tag{5.177}$$

Substituting into (5.174):

$$\boxed{\frac{d\sigma}{d\Omega} = \frac{\alpha^2}{2s}\left[\frac{1}{2}(1+\cos^2\theta) + \frac{4+(1+\cos\theta)^2}{(1-\cos\theta)^2} - \frac{(1+\cos\theta)^2}{1-\cos\theta}\right]}\,. \tag{5.178}$$

The three terms have a clear physical origin: the first is the familiar s-channel annihilation contribution (identical to $e^+e^- \to \mu^+\mu^-$), the second is the t-channel exchange (which diverges as $\theta \to 0$), and the third is the s-t interference.

Physical features. Several notable features distinguish Bhabha scattering from muon pair production:

- **Forward divergence**: The $1/t^2$ term from the t-channel causes the cross section to diverge as $\theta \to 0$ (forward scattering). This is characteristic of Coulomb scattering—the long-range nature of the electromagnetic interaction leads to a preference for small-angle scattering.
- **Interference**: The s-t interference term $2u^2/(st)$ is negative for backward scattering ($\cos\theta < 0$, where $u > 0$, $t < 0$, $s > 0$), reducing the cross section relative to the sum of s- and t-channel contributions alone.
- **Annihilation channel**: At $\theta = 90°$ ($t = u = -s/2$), all three terms contribute comparably. At high energies and large angles, the annihilation diagram becomes relatively more important.
- **Luminosity monitoring**: Despite the forward divergence, Bhabha scattering at specific angles provides a precisely calculable process used for luminosity measurements at e^+e^- colliders.

Box 5.5 Comparison with $e^+e^- \to \mu^+\mu^-$

For muon pair production, only the s-channel contributes, giving:

$$\overline{|\mathcal{M}|^2}_{e^+e^-\to\mu^+\mu^-} = \frac{2e^4(t^2+u^2)}{s^2}\,. \tag{5.179}$$

This corresponds to setting $X_{tt} = X_{st} = 0$ in the Bhabha formula. The angular distribution $(1+\cos^2\theta)$ is characteristic of spin-1 intermediate states coupling to spin-$\frac{1}{2}$ fermions. In Bhabha scattering, the additional t-channel and interference terms modify this pattern, creating the characteristic forward peak.

The forward divergence: physics and regularization

The $1/t^2$ divergence as $\theta \to 0$ deserves careful discussion. This is *not* an artifact of the calculation but reflects the physics of long-range Coulomb interactions.

Origin of the divergence. In classical mechanics, the Rutherford cross section for Coulomb scattering also diverges as $\theta \to 0$:

$$\left.\frac{d\sigma}{d\Omega}\right|_{\text{Rutherford}} = \frac{\alpha^2}{4E^2\sin^4(\theta/2)} \xrightarrow{\theta\to 0} \infty\,. \tag{5.180}$$

The divergence arises because the Coulomb potential $V(r) \sim 1/r$ has infinite range. Particles with arbitrarily large impact parameters still experience a (small) deflection, leading to an infinite total cross section. This is fundamentally different from scattering off a finite-range potential, where the cross section is finite.

Why the total cross section diverges. Integrating the differential cross section:

$$\begin{aligned}\sigma_{\text{tot}} &= \int \frac{d\sigma}{d\Omega}\,d\Omega \sim \int_0^\pi \frac{\sin\theta\,d\theta}{(1-\cos\theta)^2} \\ &\sim \int_0 \frac{d\theta}{\theta^3} \to \infty\,.\end{aligned} \tag{5.181}$$

The integral diverges at the lower limit. Physically, this means that *every* electron-positron pair in a beam "scatters" to some degree—most by unmeasurably small angles.

Regularization in practice. Several mechanisms regularize this divergence:

1. **Angular cutoff**: In any experiment, detectors have finite angular acceptance. Defining a minimum scattering angle θ_{min} renders the cross section finite:

$$\sigma(\theta > \theta_{\text{min}}) = \int_{\theta_{\text{min}}}^{\pi} \frac{d\sigma}{d\Omega}\,d\Omega < \infty\,. \tag{5.182}$$

2. **Screening**: In matter, the Coulomb potential is screened at large distances by other charges. This effectively gives the photon a small mass $m_\gamma \sim 1/\lambda_D$ (where λ_D is the Debye length), cutting off the divergence.

3. **Vacuum polarization**: At the quantum level, virtual e^+e^- pairs (and other charged particles) momentarily appear from the vacuum and modify the photon propagator. The bare propagator $1/t$ is replaced by:

$$\frac{1}{t} \to \frac{1}{t\left[1-\Pi(t)\right]}, \tag{5.183}$$

where $\Pi(t)$ is the vacuum polarization function. In renormalized QED, gauge invariance implies $\Pi(0) = 0$, so vacuum polarization does *not* remove the Coulombic $1/t$ pole in the forward direction: the photon remains massless, and the small-angle enhancement persists. The practical regularization of the forward divergence therefore comes from angular cuts, screening in matter, finite beam size, and finite detector resolution.
4. **Finite beam size**: Real beams have finite spatial extent, which limits the maximum impact parameter and thus the minimum scattering angle.

Detailed comparison: Bhabha vs. muon pair production

The structural differences between $e^+e^- \to e^+e^-$ and $e^+e^- \to \mu^+\mu^-$ provide insight into the role of channel interference and crossing structure in QED.

Channel structure.

	Bhabha ($e^+e^- \to e^+e^-$)	**Muon production** ($e^+e^- \to \mu^+\mu^-$)
s-channel	✓ (annihilation)	✓ (annihilation)
t-channel	✓ (exchange)	× (forbidden)
Interference	✓ (s-t)	×

The t-channel is forbidden in muon production because it would require an $e \to \mu$ transition, which violates lepton flavor conservation at tree level.

Angular distributions. Writing the differential cross sections explicitly:

$$\left(\frac{d\sigma}{d\Omega}\right)_{e^+e^-\to\mu^+\mu^-} = \frac{\alpha^2}{4s}(1+\cos^2\theta), \tag{5.184}$$

$$\left(\frac{d\sigma}{d\Omega}\right)_{e^+e^-\to e^+e^-} = \frac{\alpha^2}{2s}\left[\underbrace{\frac{1+\cos^2\theta}{2}}_{\text{from } s\text{-channel}} + \underbrace{\frac{4+(1+\cos\theta)^2}{(1-\cos\theta)^2}}_{\text{from } t\text{-channel}} - \underbrace{\frac{(1+\cos\theta)^2}{1-\cos\theta}}_{\text{interference}}\right]. \tag{5.185}$$

Key differences:

- **Forward region** ($\theta \to 0$): Muon production $\to \frac{\alpha^2}{2s}$ (finite); Bhabha $\to \infty$ (divergent)
- **Backward region** ($\theta \to \pi$): Both finite, but Bhabha is suppressed by destructive s-t interference
- **At** $\theta = 90°$: Muon production gives $\frac{\alpha^2}{4s}$; Bhabha gives $\frac{3\alpha^2}{2s}$ (enhanced by t-channel)

Ratio of cross sections. At large angles, the t-channel contribution becomes subdominant. To see why, recall that the t-channel amplitude scales as $1/t$ where $t = -2E^2(1-\cos\theta)$. At backward angles ($\theta \to \pi$):

$$|t| = 2E^2(1-\cos\theta) \xrightarrow{\theta\to\pi} 4E^2 = s\,. \tag{5.186}$$

Thus $X_{tt} \sim 1/t^2 \sim 1/s^2$, which is the same order as $X_{ss} \sim 1/s^2$. At backward angles, the interference term $X_{st} \sim 1/(st)$ is *destructive*, so the total Bhabha cross section remains of the same parametric order as the annihilation contribution rather than being forward-enhanced.

Defining the ratio $R(\theta) = (d\sigma/d\Omega)_{\text{Bhabha}}/(d\sigma/d\Omega)_{\mu\mu}$:

$$R(\theta) \xrightarrow{\theta\to\pi} 2 + \mathcal{O}(1+\cos\theta)\,. \tag{5.187}$$

At small angles, the ratio diverges as $R(\theta) \sim 1/\theta^4$ due to the $1/t^2$ enhancement.

Helicity amplitude analysis

The helicity structure of Bhabha scattering extends the analysis presented for $e^+e^- \to \mu^+\mu^-$ in Section 5.2. We now have two channels whose interference creates a richer helicity structure.

Review: helicity selection rules. As discussed in Section 5.2, for massless fermions helicity is conserved at QED vertices. The virtual photon couples only to $f\bar{f}$ pairs with opposite helicities. The initial state $e^-_L e^+_R$ gives $J_z = h_{e^-} - h_{e^+} = -\frac{1}{2} - \frac{1}{2} = -1$, while $e^-_R e^+_L$ gives $J_z = +1$. Configurations like $e^-_L e^+_L$ have $J_z = 0$ and do not couple to a transverse photon.

s-channel amplitudes (same as $\mu^+\mu^-$). The s-channel in Bhabha scattering has exactly the same helicity structure as muon pair production. Using the Wigner d-matrices introduced in the box of Section 5.2:

$$\mathcal{M}_s(LR \to LR) \propto \frac{e^2}{s} d^1_{-1,-1}(\theta) = \frac{e^2}{s}\frac{1+\cos\theta}{2} \tag{5.188}$$

$$\mathcal{M}_s(LR \to RL) \propto \frac{e^2}{s} d^1_{-1,+1}(\theta) = \frac{e^2}{s}\frac{1-\cos\theta}{2}\,, \tag{5.189}$$

with analogous expressions for $RL \to LR$ and $RL \to RL$ by the substitution $\theta \to \pi - \theta$ in the d-matrices.

t-channel amplitudes. The t-channel has a different helicity structure. Here, the electron and positron lines are separate—each scatters independently off the exchanged photon. Helicity is conserved along each fermion line:

- $e_L^- \to e_L^-$ (electron line preserves helicity)
- $e_R^+ \to e_R^+$ (positron line preserves helicity)

Thus the t-channel only contributes to helicity-conserving configurations:

$$\begin{aligned}\mathcal{M}_t(LR \to LR) &= \frac{e^2}{t}\,[\bar{u}_L(p_3)\gamma^\mu u_L(p_1)] \\ &\qquad \times [\bar{v}_R(p_2)\gamma_\mu v_R(p_4)] \\ &\propto \frac{e^2}{t}\cdot s \cdot \frac{1+\cos\theta}{2}\,.\end{aligned} \tag{5.190}$$

The factor $s(1+\cos\theta)/2$ arises from the spinor products. Crucially, $\mathcal{M}_t(LR \to RL) = 0$ because helicity flip is forbidden in the t-channel.

Total amplitudes and interference. For the helicity-conserving configuration $LR \to LR$, both channels contribute:

$$\mathcal{M}(LR \to LR) = \mathcal{M}_s - \mathcal{M}_t = e^2\left[\frac{1}{s} - \frac{1}{t}\right]\frac{1+\cos\theta}{2}\cdot(\text{spinor factor})\,. \tag{5.191}$$

The relative minus sign from Fermi statistics is crucial. Since $s > 0$ and $t < 0$, both terms have the *same sign*, leading to constructive interference at forward angles and destructive interference at backward angles.

For the helicity-flip configuration $LR \to RL$, only the s-channel contributes:

$$\mathcal{M}(LR \to RL) = \mathcal{M}_s = \frac{e^2}{s}\frac{1-\cos\theta}{2}\cdot(\text{spinor factor})\,. \tag{5.192}$$

Angular distribution from helicity sum. Squaring and summing over helicities (factor of 2 for $LR \leftrightarrow RL$ symmetry):

$$\sum_{\text{hel}} |\mathcal{M}|^2 = 2\left|\frac{e^2(1+\cos\theta)}{2}\left(\frac{1}{s} - \frac{1}{t}\right)\right|^2 + 2\left|\frac{e^2(1-\cos\theta)}{2s}\right|^2 + (L \leftrightarrow R)\,. \tag{5.193}$$

The first term (helicity-conserving) contains the t-channel pole and s-t interference; the second term (helicity-flip) is pure s-channel. This reproduces the trace calculation and explains the physical origin of each contribution in eq. (5.159).

Experimental applications and precision tests

Bhabha scattering plays a central role in the physics program of e^+e^- colliders, serving both as a luminosity monitor and as a probe of QED at high precision.

Luminosity determination. The integrated luminosity $\mathcal{L}$ relates the number of observed events N to the cross section σ:

$$N = \mathcal{L} \cdot \sigma \,. \tag{5.194}$$

To measure $\mathcal{L}$, one needs a process with: (i) large cross section (high statistics), (ii) clean experimental signature, and (iii) precisely calculable theoretical cross section. Small-angle Bhabha scattering satisfies all three criteria:

- The $1/t^2$ enhancement gives a large rate at small angles
- The e^+e^- final state has a distinctive back-to-back topology
- Being a pure QED process, radiative corrections are calculable to high precision

Precision at LEP. At LEP, small-angle Bhabha scattering (SABS) was measured with remarkable precision. The OPAL, ALEPH, DELPHI, and L3 experiments achieved:

- **Experimental precision**: $\sim 0.05\%$–0.08% using silicon-tungsten luminometers
- **Theoretical precision**: The Monte Carlo generator BHLUMI 4.04 achieved 0.061% at LEP1 (Z pole) and 0.122% at LEP2 (higher energies)
- **Combined uncertainty**: $\lesssim 0.1\%$ on the luminosity measurement

This precision was essential for the electroweak precision tests at LEP, where cross sections and asymmetries were measured with per-mille accuracy.

Running of α. Large-angle Bhabha scattering at LEP was used to measure the running of the QED coupling $\alpha(q^2)$. The OPAL collaboration measured $\alpha(t)$ for space-like momentum transfer, confirming the predicted logarithmic running from vacuum polarization effects.

Radiative corrections. For precision applications, higher-order corrections must be included:

1. **Virtual corrections**: One-loop vertex and box diagrams modify the amplitude at $\mathcal{O}(\alpha)$
2. **Real emission**: Bremsstrahlung $e^+e^- \to e^+e^-\gamma$ contributes when soft/-collinear photons are undetected

3. **Vacuum polarization**: Modifies the photon propagator, introducing hadronic uncertainties
4. **Weak corrections**: Z boson exchange becomes relevant near $\sqrt{s} \sim M_Z$

The complete $\mathcal{O}(\alpha)$ correction to the Bhabha cross section is typically $\sim$ 10–30%, depending on the experimental cuts. Two-loop corrections at $\mathcal{O}(\alpha^2)$ are at the per-mille level and have been computed for precision applications.

Future colliders. At proposed future e^+e^- colliders (FCC-ee, CEPC, ILC), the target luminosity precision is 10^{-4} or better. This requires:

- Complete two-loop QED calculations for SABS
- Precise treatment of initial-state radiation and beamstrahlung
- Control of hadronic vacuum polarization uncertainties
- Understanding of potential new physics contributions to the luminosity process

Numerical estimates and comparison with data

Order of magnitude of cross sections. The characteristic scale for QED cross sections is set by dimensional analysis:

$$\sigma \sim \frac{\alpha^2}{s}. \tag{5.195}$$

Using $\alpha \approx 1/137$ and the conversion factor $\hbar c \approx 197$ MeV $\cdot$ fm:

$$\sigma \sim \frac{\pi\alpha^2}{s} = \frac{\pi}{137^2} \cdot \frac{(197\ \text{MeV} \cdot \text{fm})^2}{s} \approx \frac{87\ \text{nb}}{(E_{\text{cm}}/\text{GeV})^2}. \tag{5.196}$$

Total cross section for $e^+e^- \to \mu^+\mu^-$. Integrating the differential cross section over the full solid angle:

$$\sigma_{e^+e^- \to \mu^+\mu^-} = \frac{4\pi\alpha^2}{3s} \approx \frac{87\ \text{nb}}{(E_{\text{cm}}/\text{GeV})^2}. \tag{5.197}$$

At $\sqrt{s} = 10$ GeV (typical B-factory energy): $\sigma \approx 0.87$ nb.
At $\sqrt{s} = 91$ GeV (Z pole): $\sigma \approx 10$ pb (enhanced by Z resonance).
At $\sqrt{s} = 200$ GeV (LEP2): $\sigma \approx 2.2$ pb.

Bhabha scattering cross section. The Bhabha total cross section diverges due to the forward singularity. With an angular cut $\theta > \theta_{\text{min}}$:

$$\sigma_{\text{Bhabha}}(\theta > \theta_{\text{min}}) \approx \frac{2\pi\alpha^2}{s}\left[\frac{1}{\sin^2(\theta_{\text{min}}/2)} + \frac{1}{3}(1 + \cos^2\theta_{\text{min}}) + \cdots\right]. \tag{5.198}$$

For small-angle Bhabha scattering with $\theta_{\min} = 30$ mrad at $\sqrt{s} = 91$ GeV:

$$\sigma_{\text{SABS}} \sim \frac{2\pi\alpha^2}{s \cdot \theta_{\min}^2} \approx 100\ \text{nb}\,. \tag{5.199}$$

This large cross section (compared to ~ 10 pb for $\mu^+\mu^-$) makes SABS ideal for luminosity monitoring.

Angular distribution: theory vs. experiment. Figure 5.2 shows the differential cross section as a function of scattering angle, comparing Bhabha scattering with muon pair production.

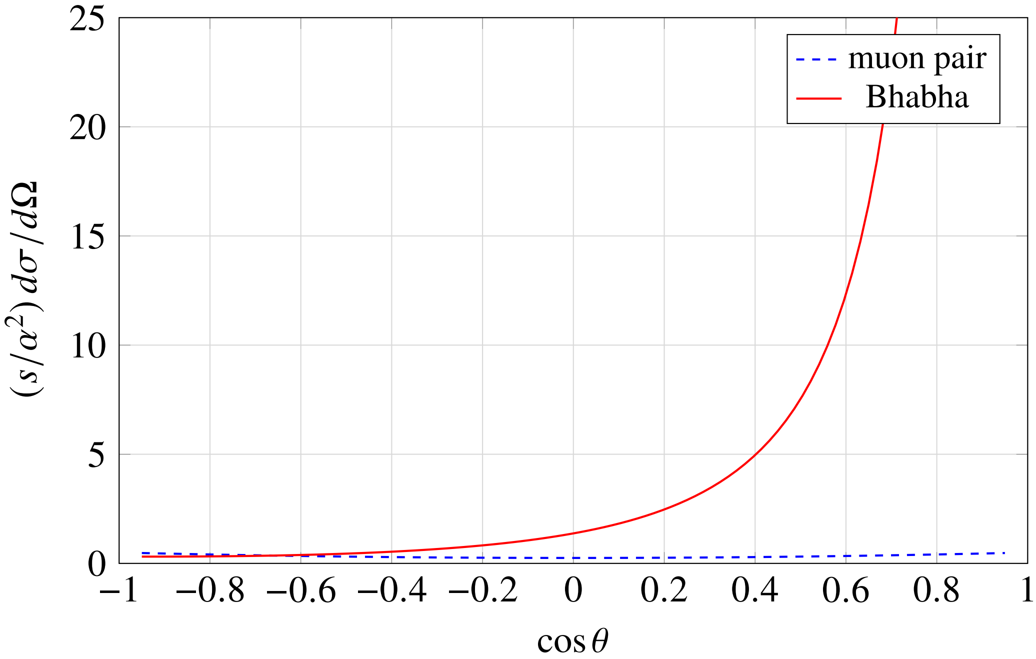

Figure 5.2. Comparison of the differential cross sections (in units of α^2/s) for Bhabha scattering ($e^+e^- \to e^+e^-$, solid red) and muon pair production ($e^+e^- \to \mu^+\mu^-$, dashed blue). The Bhabha cross section diverges as $\theta \to 0$ ($\cos\theta \to 1$) due to the t-channel pole, while muon production remains finite. At backward angles ($\cos\theta \to -1$), the two processes have similar magnitudes due to destructive s-t interference in Bhabha scattering.

Experimental verification. The Bhabha cross section has been measured with high precision at numerous e^+e^- colliders. Table 5.1 summarizes key measurements.

At LEP, the measured Bhabha cross sections agreed with QED predictions (including radiative corrections) to better than 0.1%, providing one of the most stringent tests of QED at high energies. No deviations from the Standard Model prediction were observed, setting limits on new physics such as contact interactions or extra dimensions.